Theoretical and Applied Fracture Mechanics 125 (2023) 103787

Contents lists available at ScienceDirect

Theoretical and Applied Fracture Mechanics

journal homepage: www.elsevier.com/locate/tafmec

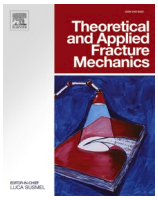

Size effect on flexural strength of notched and un-notched concrete and rock specimens by Finite Fracture Mechanics

Mattia Baldassari [a,*], Alessia Monaco [b], Alberto Sapora [a], Pietro Cornetti [a]

[a] Department of Structural, Geotechnical and Building Engineering Politecnico di Torino, C.so Duca degli Abruzzi, 24 10129 Torino, Italy
[b] Department of Architecture and Design, Politecnico di Torino, V.le Mattioli, 39 10125 Torino, Italy

ARTICLE INFO

Keywords:
Size Effect
Finite Fracture Mechanics
Three Point Bending
Semi-Circular Bending
Concrete-like materials

ABSTRACT

Size effect in quasi-brittle material cannot be described simply by Linear Elastic Fracture Mechanics, which moreover is limited to cracked geometries. In the present paper we apply Finite Fracture Mechanics to determine the size effect on the flexural strength of notched and un-notched quasi-brittle material specimens under quasi-static mode I loadings. Although the framework is general, special attention is paid on the Three Point Bending and Semi-Circular Bending test geometries. The scaling of flexural strength is of particular interest for concrete and concrete-like materials because of the large variation from laboratory to real structural sizes. Theoretical predictions are discussed and compared with several experimental data from the literature, related to both concrete and rock specimens. The excellent matching with the experimental data proves the soundness of the Finite Fracture Mechanics approach, even more valuable because of its simplicity: just two shape functions are needed to determine the scaling of the flexural strength (or of the nominal fracture toughness) for a given geometrical shape.

1. Introduction

In structural mechanics, the term size effect usually refers to the variation of the strength of a structure as its size scales proportionally. The classical continuum mechanics approach along with (local) stress failure criteria is not able to catch any size effect into account. However, scientists and engineers became soon aware of the importance of the scaling of structural strength. Of course, understanding size effects has become even more important in the last years along with the development of nanotechnologies. Thus, size effect is an ongoing key research topic, relevant both from the theoretical and the applied points of view. Quoting Bažant [1], ‘‘Scaling is a quintessential problem of every physical theory. If the scaling is not understood, a viable theory does not exist’’. Note that the source of size effect can be either statistical, deterministic, or both. Herein we focus on deterministic aspects.

About one century ago, while trying to determine the strength of a cracked structure, Griffith proposed his infinitesimal energy balance to decide whether a crack is propagating or not. It was the base for the development of the Linear Elastic Fracture Mechanics (LEFM) theory. LEFM is able to predict size effects in cracked structures because of the interplay between the stored strain energy, proportional to the volume, and the dissipated energy, proportional to the fracture surface. However, LEFM can be applied only to pre-cracked structures and to perfectly brittle materials.

For what concerns quasi-brittle materials, i.e., materials where energy during failure is mostly dissipated on crack surfaces but with an Irwin’s material length not so small with respect to specimen size, several approaches were proposed in the second half of the last century. Among them, here we can cite the Theory of Critical Distances – TCD [2,3] – and the Cohesive Crack Model – CCM [4].The basic assumption of the TCD is that failure takes place when the (linear elastic) stress at a given (material) distance from the notch tip reaches its critical value. On the other hand, CCM assumes that stress among crack faces does not drop to zero suddenly, but smoothly as the crack opening increases in the so-called process zone. TCD is appealing due to its simplicity. However, it loses accuracy as the structural size approaches the material distance. On the other hand, CCM, although accurate, is computationally expensive, requiring non-linear analyses with fine meshing in the process zone.

More recently, a new fracture model named Finite Fracture Mechanics (FFM) has been proposed, based on the assumption of a finite crack growth under proper stress and energy conditions [5]. The FFM

* Corresponding author.
E-mail address: mattia.baldassari@polito.it (M. Baldassari).

https://doi.org/10.1016/j.tafmec.2023.103787
Received 31 May 2022; Received in revised form 16 November 2022; Accepted 20 January 2023
Available online 25 January 2023

approach has proven successful since it retains the advantages of the TCD and CCM approaches (simplicity and accuracy, respectively), while overcoming their disadvantages (unreliability at small sizes and high computational costs, respectively). Furthermore, FFM turns out to be very effective in addressing size effects issues, as can be seen by a literature review. To cite but a few, here we like to mention the contributions by Leguillon et al. [5], on size effect in cross-ply glass fiber reinforced composites; by Leguillon et al. [6], on size effect in solids containing cylindrical holes; by Erçin et al. [7], extending the holed plate analysis to composite laminates; by Cornetti et al. [8], on size effect in V-notched structures under mixed mode loadings (see also Doitrand et al. [9]); by García et al. [10], on the fiber size effect in fiber–matrix debonding; by Torabi et al. [11], on holed Brazilian disks; by Gentieu et al. [12], on particle debonding; and by Chao Correas et al. [13], on fracture onset in solids containing spherical voids.

Aim of the present paper is to apply the FFM criterion to the analysis of the size effects for typical concrete testing configurations (all under mode I load conditions), extending earlier results presented in Cornetti et al. [14]. Particularly, the Three Point Bending (TPB) and the Semi-Circular Bending (SCB) test geometries will be analyzed and compared with several data from the literature related also to rock materials.

The paper is onward organized as follows: Section 2 presents the equations FFM is based on. Section 3 is devoted to the analysis of the size effect on plain specimens under pure bending. For such a geometry, the expressions of the large and small size asymptotes are derived analytically; moreover, an approximate formula providing the well-known size effect of increasing maximum flexural stress with decreasing specimen size is also given. Section 4 shows the size effect on notched and un-notched TPB specimens. Theoretical results are compared with data from the literature on concrete specimens. Section 5 is devoted to the size effect analysis of cracked SCB tests and a comparison with experimental data on rock specimens from the literature is provided. Finally, conclusions are drawn in Section 6.

Before starting, it is worth saying that the Literature about the size effect is huge, especially for what concerns concrete structures, where the difference between laboratory and real sizes is usually large and, thus, the understanding of size effect is of paramount relevance. Here we refer to the fundamental books on the subject by Bažant and Planas [15] and Bažant [16] and to references therein. Note that size effect laws claiming universality have been proposed in the past, like the Size Effect Law by Bažant [17], the Multi Fractal Scaling Law by Carpinteri et al. [18] or the asymptotic size effect analysis by Karihaloo [19]. All these laws are based on parameters that have to be fitted for any specific geometry. In the present work the goal is less ambitious, since we restrict the investigation on the size effect on the flexural strength of notched and un-notched specimens. On the other hand, the only parameters needed are the fracture energy and tensile strength, i.e., material parameters with a clear physical meaning. Note that this latter feature is shared by the Boundary Effect Model, originally proposed by Hu and Wittmann [20] to take the effect of process zone lengths close to the ligament width into account, and then deeply investigated and improved (see e.g. Guan et al. [21–23]) to include the effect of the maximum grain size on concrete and rock fracture.

2. Finite Fracture Mechanics

As mentioned in the Introduction, local strength criteria along with linear elasticity are not able to predict any size effect as for lacking any internal length. One of the simpler ways to overcome such a drawback is requiring the stress to be higher than material strength σ_c not just at the crack onset point, but over a region (a length in 2D geometries), in order to have failure. Referring to Fig. 1a, we can, for instance, impose that the stress exceeds the tensile strength ahead the crack tip over the length Δ upon failure:

$$\sigma_y(x) \geqslant \sigma_c, \quad 0 < x < \Delta \tag{1}$$

Alternatively, we can demand the average stress to exceed the tensile strength, i.e.:

$$\int_0^{\Delta} \sigma_y(x)\mathrm{d}x \geqslant \sigma_c \Delta \tag{2}$$

In order Eqs. (1) and (2) to provide the same LEFM predictions for sufficiently large cracks, it is easy to check that Δ must be equal to $(1/2\pi)\ l_{ch}$ and $(2/\pi)\ l_{ch}$ respectively, l_{ch} being Irwin's (characteristic) length of the material $(K_{Ic}/\sigma_c)^2$ and K_{Ic} the material fracture toughness (Taylor [3]; Louks et al.[24]).

Eqs. (1) and (2) are the base of TCD. Although in several cases they work pretty well, they lack a clear physical background and, most important, TCD predictions become unreliable as the material length and the ligament size get comparable. Considering, for instance, a geometry where the stress resultant over the ligament is null (like in bending, see Fig. 2), Eq. (2) clearly provides an infinite failure load for a ligament length equal to (or lower than) $(2/\pi)\ l_{ch}$.

In order to overcome such a shortcoming and, at the same time, to provide a deeper physical meaning to non-locality, either Eq. (1) or (2) have been coupled with the discrete energy balance for finite crack growth, leading to FFM fracture criterion (sometimes also called Coupled Criterion). Accordingly, the crack advance Δ is no longer a material property and the actual failure load is the minimum among the ones satisfying the following inequalities [5]

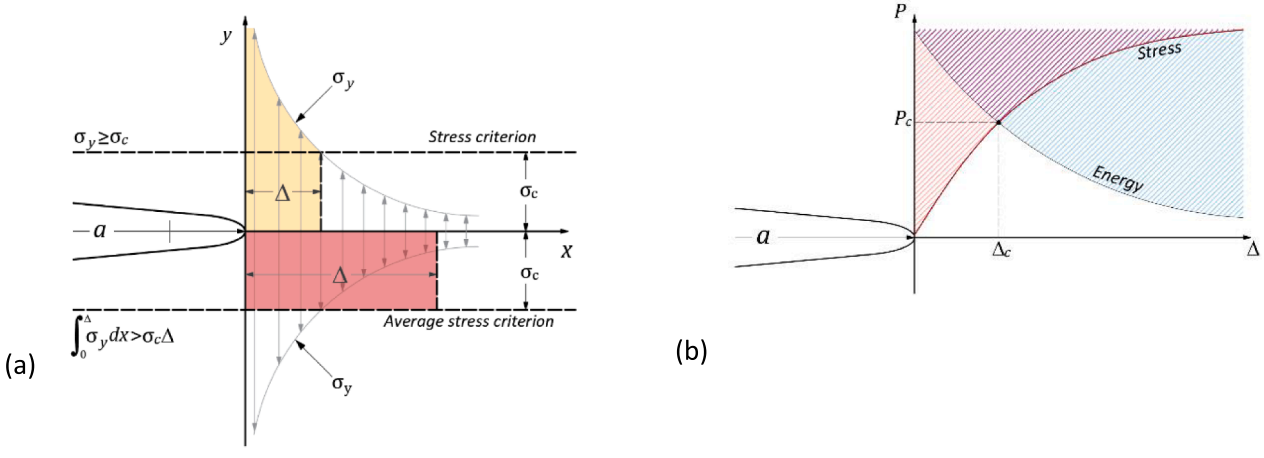

Fig. 1. TCD (a) and FFM (b) reference schemes.

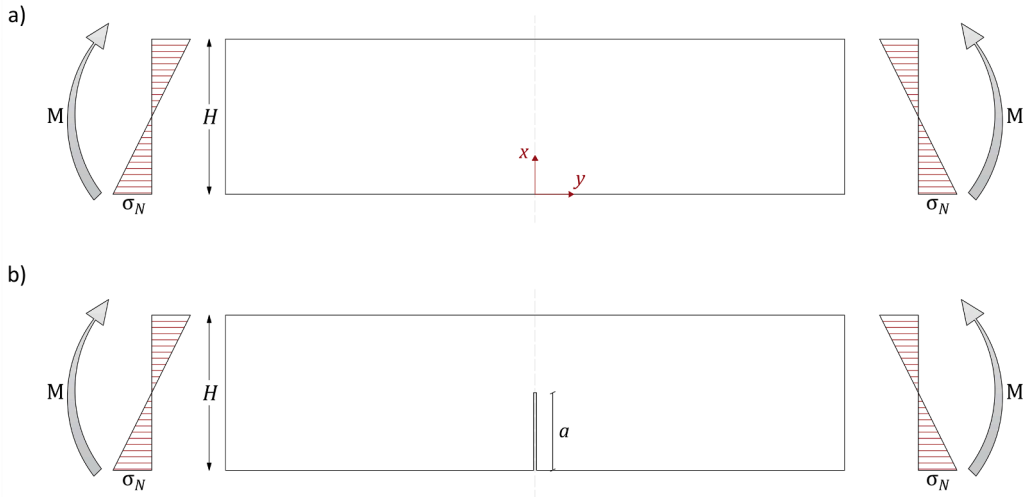

Fig. 2. Pure bending: plain specimen (a); cracked specimen (b).

$$\begin{cases} \sigma_y(x) \geqslant \sigma_c \ , & 0 < x < \Delta \\ \displaystyle\int_a^{a+\Delta} G(a')\,\mathrm{d}a' \geqslant G_c\Delta \end{cases} \tag{3}$$

where Eq. (1) has been chosen as stress condition and the second equation implies that the energy available for crack growth from a to $a+\Delta$ must exceed the energy $G_c\Delta$ needed to create the new fracture surface, G_c being the material fracture energy. Alternatively, opting for Eq.(2), one gets [14]:

$$\begin{cases} \displaystyle\int_0^{\Delta} \sigma_y(x)\mathrm{d}x \geqslant \sigma_c\Delta \\ \displaystyle\int_a^{a+\Delta} G(a')\mathrm{d}a' \geqslant G_c\Delta \end{cases} \tag{4}$$

Let us now focus on Eq. (4). The integrand function in the first equation is usually monotonically decreasing, whereas the integrand function in the second one is generally monotonically increasing (in this case the geometry is named *positive*, and cases considered herein will fall in this class). It follows that the former inequality is satisfied for loads P increasing with Δ while the latter one for loads decreasing with Δ (see Fig. 1b). Thus, the minimum load satisfying Eq. (4) is the one for which both inequalities are strictly fulfilled. On the basis of this consideration and of Irwin's relationship, we can recast Eq.(4) in terms of Stress Intensity Factor (SIF, K_I) and fracture toughness K_{Ic} as:

$$\begin{cases} \displaystyle\int_0^{\Delta} \sigma_y(x)\,\mathrm{d}x = \sigma_c\Delta \\ \displaystyle\int_a^{a+\Delta} K_I^2(a')\mathrm{d}a' = K_{Ic}^2\Delta \end{cases} \tag{5}$$

Eq. (5) is a system of two equations in two unknowns, P and Δ, P being implicitly embedded in $\sigma_y(x)$ and $K_I(a)$ functions. Its two solutions provide the actual crack advance Δ_c and corresponding failure P_c (see Fig. 1b).

Note that, as the CCM can be implemented by means of different cohesive laws, analogously FFM can be used by implementing different stress requirements [25]. In the following we will use the average stress condition (and, thus, Eq. (5)) since, in comparison to Eq. (3), it provides a milder size effect on flexural strength which usually better agrees with the experimental data on concrete and rock specimens (see Appendix A).

3. Pure bending of plain specimens

As a first example of the capabilities of the FFM approach to detect size effects on the strength of a structure, let us consider the case of pure bending of an un-notched beam with a rectangular cross section (Fig. 2a). The stress field over a generic cross section is given by elementary beam theory as:

$$\sigma_y(x) = \sigma_N(1 - 2x/H) \tag{6}$$

being σ_N the (maximum) normal stress at the beam intrados. According to the simple maximum normal stress criterion, failure is expected whenever σ_N reaches the material tensile strength, i.e., $\sigma_{N,f} = \sigma_c$ whatever the structural size H is. However, it is well known that $\sigma_{N,f}$ increases as the structural size decreases (see e.g., Doitrand et al. [26]). We will show that FFM is able to catch such an effect and will derive it.

For brittle materials, the specimen is expected to fail by a vertical crack starting from the beam intrados (Fig. 2b). A highly accurate expression (error less than 1% for any relative crack depth) for the SIF for such a crack is provided by Guinea et al. [27]:

$$K_I = \sigma_N\sqrt{H}\,f_{k\infty}(\alpha) \tag{7}$$

where:

$$f_{k\infty}(\alpha) = \frac{\sqrt{\alpha}}{(1-\alpha)^{3/2}(1+3\alpha)}\ \ p_\infty(\alpha) \tag{8}$$

$$p_\infty(\alpha) = 1.99 + 0.83\alpha - 0.31\alpha^2 + 0.14\alpha^3 \tag{9}$$

and $\alpha = a/H$ is the relative notch depth, i.e., the ratio between the crack depth and the specimen height. The symbol ∞ is used because pure bending can be seen as the limit case of TPB when the beam slenderness tends to infinity. We can now substitute Eqs. (6) and (7) into the FFM system (5). Simple analytical manipulations lead to:

$$\begin{cases} \dfrac{\sigma_N}{\sigma_c} = \dfrac{1}{1-\delta} \\ \left(\dfrac{\sigma_N}{\sigma_c}\right)^2 = \dfrac{\delta}{\rho\displaystyle\int_0^{\delta} f_{k\infty}^2(\alpha)\mathrm{d}\alpha} \end{cases} \tag{10}$$

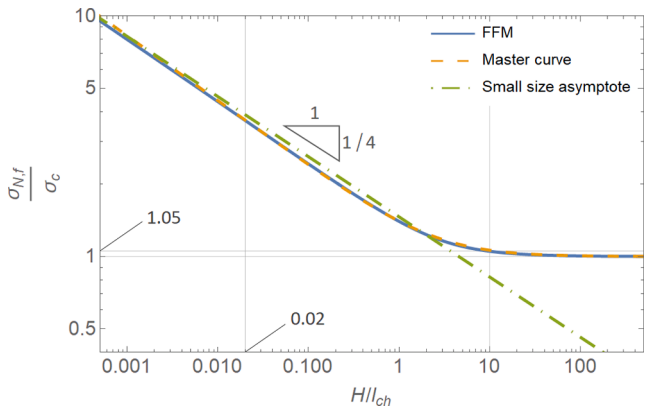

Fig. 3. Size effect on flexural strength of plain specimens: bi-logarithmic plot.

where $\rho = H/l_{ch}$ is the dimensionless size and $\delta = \Delta/H$ is the dimensionless discrete crack increment. For a given size (i.e., a given ρ), the discrete crack increment is achieved by squaring the first equation and equating the right-hand sides:

$$\delta(1-\delta)^2 = \rho \int_0^\delta f_{k\infty}^2(\alpha)\mathrm{d}\alpha \tag{11}$$

Once the root $\delta = \delta_c$ of Eq. (11) is (numerically) computed, its substitution into either the first or the second equation of the system (10) provides the failure load, i.e., the critical nominal stress $\sigma_{N,f}$.

However, if we are interested just in the size effect, there is no need to solve Eq. (11). In fact, from the second equation of the system (10), we can explicit ρ as a function of δ and $\sigma_{N,f}/\sigma_c$. By the first equation, $\sigma_{N,f}/\sigma_c$ can then be expressed as a function of δ, so that we finally get:

$$\begin{cases} \rho(\delta) = \dfrac{\delta(1-\delta)^2}{\displaystyle\int_0^\delta f_k^2(\alpha)\mathrm{d}\alpha} \\ \dfrac{\sigma_{N,f}}{\sigma_c}(\delta) = \dfrac{1}{1-\delta} \end{cases} \tag{12}$$

Eq. (12) represents the size effect on the nominal failure stress (i.e., the flexural strength) expressed in dimensionless parametric form and it is plotted in Fig. 3; the parameter is δ and it can vary within the range $0 < \delta < 1$.

Looking at Fig. 3, it is clear that the nominal strength has two asymptotes in the bi-logarithmic diagrams. The one for large sizes is obviously horizontal, represented by the material tensile strength. For small sizes ($\rho \to 0$), the asymptote is slant, with a slope $-1/4$. That is, $\sigma_{N,f}/\sigma_c = d\rho^{-0.25}$. In order to prove analytically this result and, at the same time, to determine the constant d, we need to solve the following limit:

$$d^4 = \lim_{\delta\to 1^-}\left[\rho\left(\frac{\sigma_{N,f}}{\sigma_c}\right)^4\right] = \lim_{\delta\to 1^-}\frac{\delta/(1-\delta)^2}{\int_0^\delta f_k^2(\alpha)\mathrm{d}\alpha} \tag{13}$$

where we used Eq. (12). Both numerator and denominator diverge as $\delta \to 1^-$. By de l'Hôpital rule we can remove the singularity. Then, by Eqs. (8) and (9):

$$d^4 = \lim_{\delta\to 1^-}\frac{(1+\delta)/(1-\delta)^3}{f_k^2(\delta)} = \lim_{\delta\to 1^-}\frac{(1+\delta)(1+3\delta)^2}{\delta\, p_\infty^2(\delta)} = \frac{32}{p_\infty^2(1)} = 4.56 \tag{14}$$

That is, $d = 1.46$. Hence the asymptotes of the size effect curve are:

$$\sigma_{N,f} = \sigma_c\,, \qquad H\to\infty \tag{15a}$$

$$\sigma_{N,f} = 1.46\frac{\sqrt{K_{Ic}\sigma_c}}{\sqrt[4]{H}}\,, \qquad H\to 0 \tag{15b}$$

and are plotted in Fig. 3. Note that, while the overall solution is just approximate (yet highly accurate), being based on the polynomial interpolating function Eq. (9), the small size effect slope $-1/4$ is an exact result: it follows (beyond from the FFM approach) from the singular behavior of the SIF for a vanishing ligament (here ruled by the term $(1-\alpha)^{3/2}$ at denominator in Eq. (8)).

Fig. 3 shows that, from an engineering point of view, the size effect on the flexural strength becomes negligible for specimen heights larger than ten times Irwin's length, since the nominal strength increment is less than 5% of the asymptotic value σ_c when $H > 10\, l_{ch}$. On the other hand, for small sizes the size effect curve approaches its asymptote from below. This relatively odd behavior makes the small size asymptote provide accurate nominal strength values only for very small sizes and, thus, Eq.(15b) is of little help.

The crack advance normalized with respect to the specimen height and the material length are reported in Fig. 4a and 4b, respectively. These graphics show that the finite crack increment Δ tends to cover the whole ligament H for small sizes, whilst for large sizes Δ tends to the value $2l_{ch}/(\pi c^2)$, with $c = 1.1215$. This value can be achieved analytically by observing that, for large un-cracked size, the SIF to be inserted in the discrete energy balance approaches the expression $K_I = c\,\sigma_N\sqrt{\pi a}$.

It is noteworthy to observe that the small size limit $\Delta = H$ is just a structural parameter, whereas the large size limit $\Delta = 2l_{ch}/(\pi\, c^2)$ is just dependent on the material. In all the intermediate cases, the finite crack growth (and the corresponding strength) depends on both material and geometry.

Following an approach similar to that given in Doitrand et al. [26], here we introduce a *master curve*, i.e., an analytical expression approximating the FFM solution, as:

$$\sigma_{N,f} = \sigma_c\left(1 + \frac{2.5\, l_{ch}}{H}\right)^{0.27} \tag{16}$$

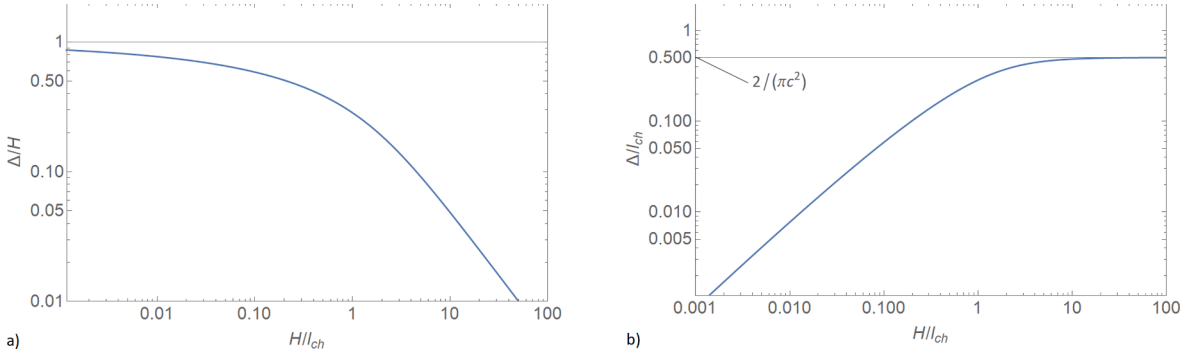

Fig. 4. Finite crack advance normalized with respect to the ligament (a); Finite crack advance normalized with respect to the characteristic length (b).

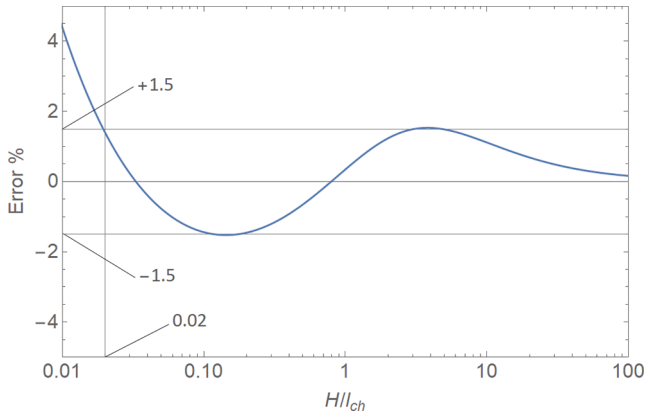

Fig. 5. Percentage error between flexural strength predicted by the master curve - Eq. (16) - and the FFM solution - Eq. (12) - vs dimensionless size.

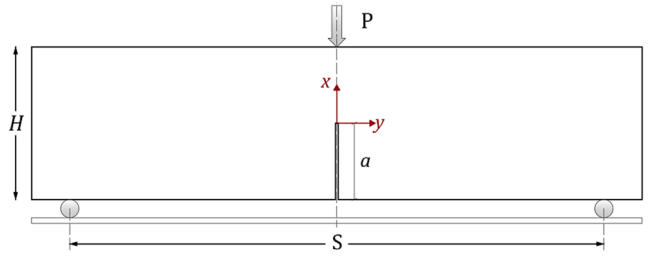

Fig. 6. TPB test set-up specimen.

Eq. (16) provides the size effect on the flexural strength with an error in comparison to the FFM solution lower than 1.5% (see Fig. 3 and Fig. 5) for any specimen height $H > 0.02\, l_{ch}$, a range that is supposed to cover most of the engineering applications. By testing at least two different sizes, the master curve by Eq. (16) can provide an estimate of the *true* material tensile strength starting from the experimental *size-dependent* flexural strength.

4. Three point bending test

In the present section the FFM coupled criterion presented in Section 2 is applied to the TPB geometry. Both plain and cracked specimens are considered. Attention is focused on the size effect. Comparison with four sets of experimental data from the scientific literature on concrete specimens is then provided.

4.1. Finite Fracture Mechanics

Let us consider a TPB specimen as in Fig. 6: H is the specimen height, S is the span (i.e., the distance between the supports), B the thickness and a the crack depth. We further introduce the slenderness β, defined as the ratio between the span and the height (i.e., $\beta = S/H$).

By suitable interpolation of the solutions for pure bending ($\beta \to \infty$, given in the previous section) and for slenderness equal to four ($\beta = 4$), Guinea et al. [27] provided the following expression for the SIF:

$$K_I = \sigma_N \sqrt{H}\, f_k(\alpha, \beta) \tag{17}$$

where $\sigma_N = (3PS)/(2BH^2)$ is the nominal stress, i.e., the stress at the beam intrados at mid-span according to elementary beam theory and in absence of a crack. The shape function f_k is given by:

$$f_k(\alpha, \beta) = \frac{\sqrt{\alpha}}{(1-\alpha)^{3/2}(1+3\alpha)} \left\{ p_\infty(\alpha) + \frac{4}{\beta}\left[p_4(\alpha) - p_\infty(\alpha)\right] \right\} \tag{18}$$

where the polynomial function $p_\infty(\alpha)$ is the one given in Eq. (9) while $p_4(\alpha)$ is:

$$p_4(\alpha) = 1.9 + 0.41\alpha + 0.51\alpha^2 - 0.17\alpha^3 \tag{19}$$

Guinea et al. [27] claim that Eq. (18) can be used with high accuracy for any crack depth and for any slenderness $\beta > 2.5$. By means of Finite Element Analyses (FEA), we checked that it can be successfully applied also to less slender geometries ($2 < \beta < 2.5$), the error with respect to numerical values being always less than 1%.

Eq. (17) allows a straightforward implementation of the discrete energy balance. In order to set the average stress requirement, also the stress field ahead the crack tip is needed. This task is achieved by linear elastic FEAs (one for each relative crack depth). Since, for notched specimens, the stress field is singular, numerical problems could arise when performing the integral of the stress ahead the crack tip. However, the problem is easily bypassed by isolating the singular part that, by means of the SIF expression previously introduced, can be both expressed and integrated analytically. In formulae:

$$\sigma_y(x) = \frac{K_I}{\sqrt{2\pi x}} + \sigma_N f_\sigma(\alpha, x/H) \tag{20}$$

where f_σ is the stress shape function to be evaluated by proper FEAs, representing in dimensionless form the difference between the actual stress field and the asymptotic one. From LEFM theory we know that $\lim_{x\to 0} f_\sigma = 0$ [28] and, thus, a mesh refinement around the crack tip is generally not needed. By means of Eq. (17) and introducing the dimensionless variable $\xi = x/H$, Eq. (20) can be re-written as:

$$\sigma_y(\alpha, \xi) = \sigma_N \left[\frac{f_k(\alpha)}{\sqrt{2\pi\xi}} + f_\sigma(\alpha, \xi) \right] \tag{21}$$

where, for the sake of simplicity, we drop the dependence on β. We can now substitute Eq. (21) and Eq. (17) into the system (5). By using the same notation exploited in the previous section, simple analytical manipulations lead to:

$$\begin{cases} \dfrac{\sigma_N}{\sigma_c} = \dfrac{\delta}{f_k(\alpha)\sqrt{2\delta/\pi} + \displaystyle\int_0^\delta f_\sigma(\alpha, \xi)\, d\xi} \\ \left(\dfrac{\sigma_N}{\sigma_c}\right)^2 = \dfrac{\delta}{\rho \displaystyle\int_\alpha^{\alpha+\delta} f_k^2(\alpha')d\alpha'} \end{cases} \tag{22}$$

It is worth observing that Eq. (22) holds for both cracked and un-cracked geometries. In the latter case, $\alpha = 0$ and the first term at denominator in the first equation vanishes. Note also that Eq. (22) includes Eq. (10) i.e., the pure bending case analyzed in the previous section ($\alpha = 0$ and $\beta = \infty$).

The discrete crack increment is achieved by squaring the first equation and equating the right-hand sides in Eq. (22). Its substitution into either the first or the second equation of system (22) yields the failure load. However, as we saw in Section 3, if we are interested just in the size effect, it is more effective providing ρ and $\sigma_{N,f}/\sigma_c$ as a function of δ. This leads to:

$$\begin{cases} \rho(\delta) = \dfrac{\left[f_k(\alpha)\sqrt{2\delta/\pi} + \displaystyle\int_0^\delta f_\sigma(\alpha, \xi)\, d\xi \right]^2}{\delta \displaystyle\int_\alpha^{\alpha+\delta} f_k^2(\alpha')d\alpha'} \\ \dfrac{\sigma_{N,f}}{\sigma_c}(\delta) = \dfrac{\delta}{f_k(\alpha)\sqrt{2\delta/\pi} + \displaystyle\int_0^\delta f_\sigma(\alpha, \xi)\, d\xi} \end{cases} \tag{23}$$

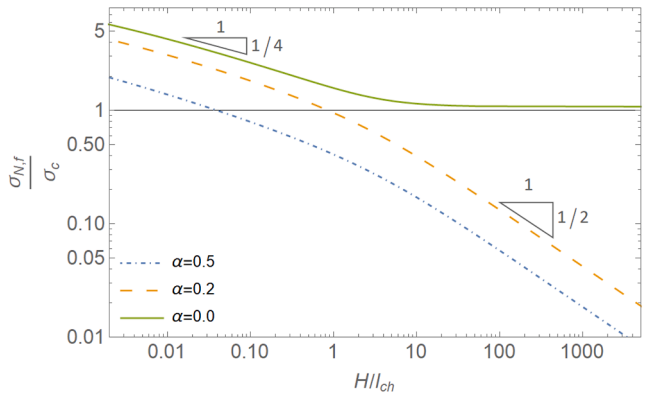

Fig. 7. Size effect for TPB specimens with slenderness $\beta = 2.5$ and different relative crack depths ($\alpha = 0, 0.2, 0.5$): bi-logarithmic plot.

For a given geometry (i.e., for given α and β values), Eq. (23) represents the size effect curve of the flexural strength $\sigma_{N,f}$ expressed in dimensionless parametric form. The parameter is the dimensionless finite crack advance δ, spanning from 0 (very large sizes) to $1 - \alpha$ (very small size), when the crack advance tends to cover the whole ligament. Eq. (23) clearly shows that, according to the FFM approach, the knowledge of the two shape functions f_σ and f_k are enough to determine the whole size effect curve.

In Fig. 7 we plot the FFM predictions for $\beta = 2.5$ and $\alpha = 0, 0.2, 0.5$, while in Fig. 8a we plot the finite crack advance normalized with respect to the ligament (i.e., $\Delta/(H - a) = \delta/(1 - \alpha)$) and in Fig. 8b the finite crack advance normalized with respect to the characteristic length (i.e., $\Delta/l_{ch} = \delta \times \rho$) for the same β and α values. All plots are bi-logarithmic ones in order to highlight the structural behavior over a wide range of scales and the power laws ruling the size effects.

For what concerns the size effect on the failure stress, Fig. 7 shows that the FFM approach predicts a transition from convexity to concavity for the size effect curve when passing from un-notched to notched geometries, similarly to what predicted by the universal size-effect law proposed by Bažant and Li [29]. The large size asymptote is in fact slant for notched specimens, corresponding to the LEFM solution (hence with a slope equal to −0.5), and horizontal for un-notched specimen, corresponding to the material tensile strength. On the other hand, for small sizes all curves present the same slope −0.25. This latter result can be proven in a way similar to the one we provided in Section 3 and, thus, we skip here analytical details for the sake of simplicity.

For what concerns the size effect on the finite crack advance, Fig. 8a shows that all the curves tend to unity as the size tends to zero, meaning that in the small size limit the crack advance tends always to cover the whole ligament. On the other hand, the large size asymptote is a decreasing straight line with slope −1, meaning that the finite crack increment tends to a constant value. The value of such a constant is made clear in Fig. 8b, where one can see that the flat large size asymptotes correspond to $\Delta = (2/\pi)\ l_{ch}$ for cracked specimens and to $\Delta = [2/(\pi\ c^2)]\ l_{ch}$, with $c = 1.1215$, for un-cracked geometries.

Before moving to the comparison with experimental results, it is worth noting that size effects can be achieved also by different models. The most popular and closest to FFM is probably the CCM [4] which is based on similar assumptions and the same material parameters. This model is widely adopted in FEAs aimed at studying the failure mechanisms of reinforced concrete and steel–concrete hybrid beams (among others, see Ballarini et al. [30–31]), where the laboratory test execution is difficult at the structural element scale for high size beams (Colajanni et al.[32]). Quite often FFM and CCM provide close results [33]; however, a detailed comparison with CCM is out of the scope of the present work. Here we want to stress that CCM provides for TPB tests always a flat small size asymptote (see e.g., Carpinteri [34]), differently from FFM, which provides a slant one. The other important aspect to be stressed is that CCM is much more burdensome, requiring a numerical non-linear analysis of crack propagation along with a fine discretization of the process zone. Actually, if one is interested just on the maximum (failure) load, some simplifications are possible, as outlined by Li and Bažant [35], where the Authors fixed the process zone size at the maximum load and then determined the corresponding structural size by solving a proper eigenvalue problem. By the way, this strategy is somewhat similar to the one followed here, where, instead of solving Eq. (22), we fix the finite crack increment and determined the corresponding size and failure load by Eq. (23). However, as far as the main goal is the maximum load, it is clear that FFM estimates are by far easier to achieve than the CCM ones. In the following section we will show that they nicely capture the experimental values too.

4.2. Comparison with experimental data

The proposed model is compared with size effect data on concrete flexural strength available in the literature in order to check its soundness and applicability. Particularly, we consider four datasets (Karihaloo et al. [19], Grégoire et al. [36], Hoover et al. [37], Çağlar and Şener [38]). In Table 1 we list all the experimental datasets considered, along with kind of tests, materials and material properties (tested or estimated).

Before entering into details of each experimental dataset, it is worth noting that we model the notched specimens as if they are cracked. Of course, the notch widths w are not null, spanning from 0.6 mm for the specimens evaluated by Hoover et al. [37] to 4 mm for the ones tested by Çağlar and Şener [38], see Table 1. However, previous studies (e.g., Carpinteri et al. [39]) showed that the effect of the radius of curvature (about one half of the notch width) at the notch tip becomes negligible

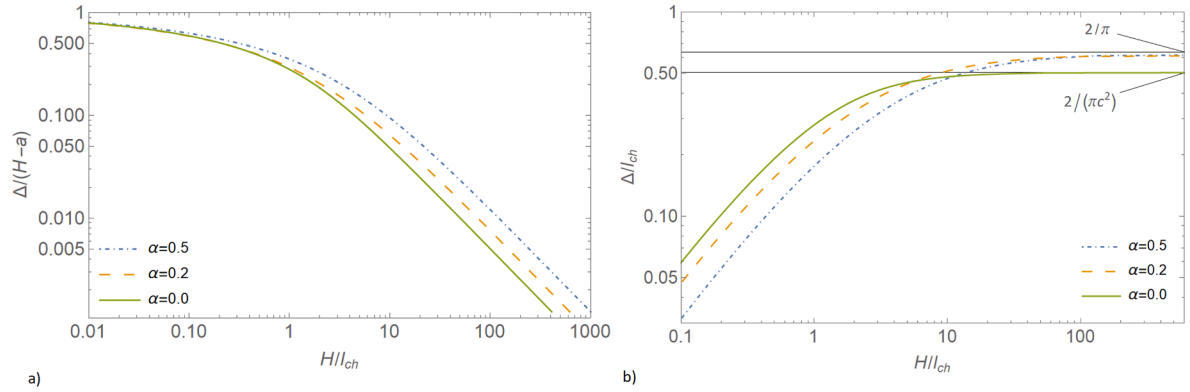

Fig. 8. Finite crack advance normalized with respect to the ligament length vs structural size (a). Finite crack advance normalized with respect to the characteristic length vs structural size (b) $\beta = 2.5$.

Table 1
Material parameters for the different experimental datasets considered.

Test and material properties							
Reference	Material	Test	σ_c [MPa]	K_{Ic} [MPa$\sqrt{m}$]	l_{ch} [mm]	w [mm]	$(w/2)/l_{ch}$ [–]
[19]	HSC	TPB	7.40[a]	1.55[b]	43.9	–	–
[36]	Concrete	TPB	3.9[a]	1.1[b]	79	2.0	1.3 %
[37]	Concrete	TPB	4.75[b]	1.11[b]	54.8	1.5	1.4 %
[38]	Concrete	TPB	4.50[b]	1.07[b]	56.0	4.0	3.6 %
[41]	Marble	SCB	11.4 [a]	1.54[b]	18.2	1.6	4.4 %
[41]	Granite	SCB	9.50 [a]	1.27[b]	17.9	1.8	5.0 %
[41]	Limestone	SCB	5.40 [a]	1.04[b]	36.7	1.9	2.6 %

[a] by split test;
[b] by best fit.

as the radius is smaller than 10% of Irwin's length l_{ch}. Since some material properties are estimated by a best fit procedure, we are able to check the requirement on the notch width only at the end of theoretical–experimental comparison. Actually, it is fulfilled by all the datasets (see again Table 1, last column), thus post-proving the validity of crack modelling assumption.

Finally, note that, since none of the investigated experimental datasets reported the concrete fracture toughness K_{Ic}, all the toughness values (summarized in Table 1) have been obtained by best fit. However, a large number of studies on K_{Ic} (along with its dependence on water-to-cement ratio, compressive strength and aggregate size) were conducted in earlier years and can be found collected in the comprehensive paper by Bažant and Becq-Giraudon [40]. Typical fracture toughness values fall within the 0.55–1.55 MPa$\sqrt{m}$ range, possibly increasing up to 2.50 MPa$\sqrt{m}$ in case of high strength concrete. Such values agree pretty well with those here obtained by best fit (see Table 1, fifth column).

4.2.1. Data by Karihaloo et al. [19]

The first experimental dataset we are considering is by Karihaloo et al. [19]. They tested High Strength Concrete (HSC) specimens. All tested specimens had a slenderness β equal to 4 and a thickness equal to 10 cm. Different relative crack depth α were considered: namely, 0%, 5%, 10% and 30%. The smallest height was 50 mm for a plain specimen and the largest 400 mm for plain and cracked specimens (except for α = 30%). The overall number of geometries tested was 15. Except for some un-cracked specimens, three specimens were evaluated per geometry. However, just the average values were reported in the paper.

Moreover, some standard tests were performed in order to characterize the material. Particularly, the Authors evaluated the tensile strength by cylindrical splitting tests, yielding a value equal to 7.40 MPa. In order to compare FFM theoretical predictions and experimental data, the material tensile strength and fracture toughness are needed. In this case, we assume the splitting strength as the reference value for the material tensile strength, i.e., $\sigma_c = 7.40$ MPa. The latter is obtained by a least squares best fit procedure, yielding a fracture toughness value $K_{Ic} = 1.55$ MPa$\sqrt{m}$.

According to these values, the comparison is provided in Fig. 9 as a dimensionless plot: the excellent agreement between theory and experiments is evident, FFM being able to catch properly the trend both for cracked and un-cracked specimens. Alternatively, one can use the experimental data to determine both tensile strength and fracture toughness, since the number of geometries and sizes is large. Proceeding in this way we get a minimization problem in two variables with a clearly defined minimum at $\sigma_c = 7.20$ MPa and $K_{Ic} = 1.60$ MPa$\sqrt{m}$, yielding a slightly better fit of experimental data. The almost coincidence of the two pairs of values (for one-parameter and two-parameter fittings) proves once more the soundness of the present approach.

4.2.2. Data by Grégoire et al. [36]

The second experimental dataset we are considering is by Grégoire et al. [36]. They tested concrete specimens (ready-mix concrete mixture obtained from Unibéton for paving slab applications). All specimens had

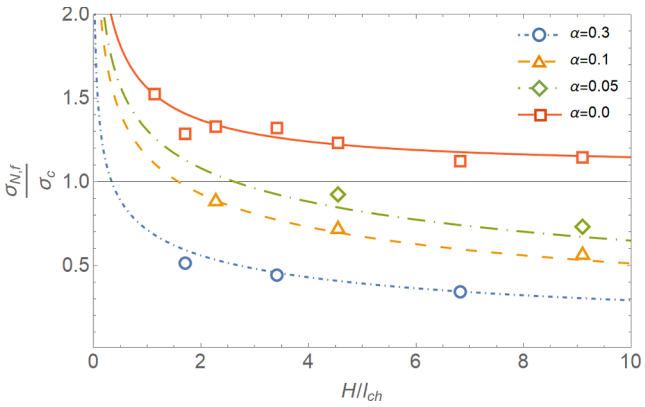

Fig. 9. Flexural strength vs specimen size for various relative crack depths: comparison with experimental data on HSC specimens obtained by Karihaloo et al. [19]. Lines refer to FFM predictions, markers to the average values of experimental data.

a slenderness β equal to 2.5 and a thickness equal to 50 mm. Four different sizes were selected so that one size is twice the previous one, yielding a size-scale range 1:8. The smallest and largest specimen heights were 50 to 400 mm. Three different relative crack depth α were chosen, respectively equal to 0%, 20% and 50%, yielding 12 different geometries tested. Three specimens were tested for (almost) each geometry, the total number of tested specimens being 34. From the same batch the Authors obtained cylindrical specimens that were used to characterize the material: particularly, a splitting strength equal to 3.9 MPa was found.

As for the former, in order to perform the comparison between FFM and experimental data, we take, as material tensile strength, the one given by the splitting test, i.e., $\sigma_c = 3.9$ MPa, and performe a least square minimization to achieve the material fracture toughness, finding $K_{Ic} = 1.1$ MPa$\sqrt{m}$. According to these values the comparison is shown in Fig. 10: the agreement is more than satisfactory, FFM predictions somewhat overestimating the size effect for cracked configurations.

A slightly better matching can be achieved by determining both tensile strength and fracture toughness by least squares method (i.e., by a two-parameter fitting), leading to the following pair of values: $\sigma_c = 4.3$ MPa, $K_{Ic} = 1.0$ MPa$\sqrt{m}$. However, also in this case difference between the values achieved by one- or two-parameter best fitting is rather small.

4.2.3. Data by Hoover et al. [37] and by Çağlar & Şener [38]

The third and fourth experimental datasets we consider were performed by Hoover et al. [37] and Çağlar & Şener [38]. Although the data refer to two completely independent experimental campaigns, geometry and sizes tested were exactly the same. Both the researcher teams tested concrete (ready-mix concrete mixture) TPB specimens with several different relative notch depth α (0%, 2.5%, 7.5%, 15% and 30%). Heights

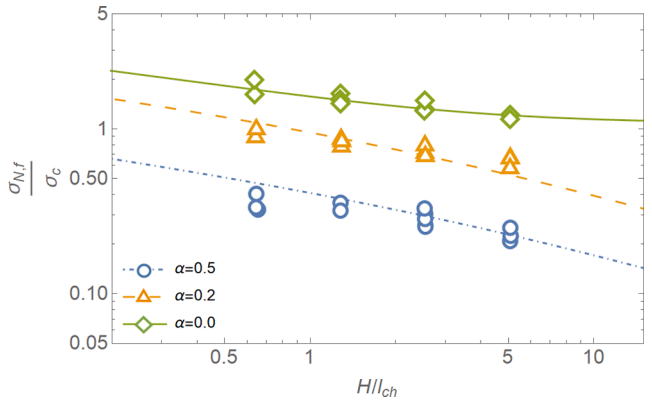

Fig. 10. Nominal failure stress vs specimen size for various relative crack depths (bi-logarithmic plot): comparison with experimental data on concrete specimens obtained by Grégoire et al. [36]. Lines refer to FFM predictions, markers to experimental data.

H were 40, 93, 215 and 500 mm, thus covering more than one order of magnitude between smallest and largest size (size range 1:12.5). For all the beams, thickness was 40 mm, and the span-to-depth ratio β was 2.176. Thus, the total number of tested geometries is 20. A total of 128 specimens (6 per type, plus some extra specimens for smaller sizes in which scatter is greater) were tested by Hoover et al. [37], after 400 days of curing, under wet burlap, in a curing room of 100% humidity and temperature about 25 °C. Regarding Çağlar & Şener [38], tested specimens were 80 (4 per geometry type), cured for 200 days under wet burlap at room temperature and humidity.

In both the experimental campaigns, the Authors did not perform tensile split tests. Actually, Hoover et al. [38] evaluated the flexural strength according to standards. However, flexural strength is usually rather larger than split tensile strength; thus, we opt for a two-parameter least squares fitting procedure, here even more justified by the vast number of geometries tested . The following pairs of material parameters are clearly identified: σ_c =4.75 MPa, K_{Ic} = 1.11 MPa$\sqrt{m}$ for Hoover's data; σ_c = 4.50 MPa, K_{Ic} = 1.07 MPa$\sqrt{m}$ for Çağlar & Şener's results (see Table 1). Results are plotted in Fig. 11 in a bi-logarithmic form, where we split the data according to the relative crack depth given the large number of considered geometries. Note that, since the graphics are in normalized form, both datasets can be reported on the same plots. The excellent matching between theory and experiments is evident for both datasets. Just some theoretical predictions for plain (α = 0%, Fig. 11e) and shallow (α = 2.5%, Fig. 11d) notches by Çağlar & Şener [38] differ significantly from experimental data. The non-monotonic trend with the size (Fig. 11d), however, highlights some peculiarity requiring extra information to be modelled.

5. Semi-Circular bending test

In this section FFM is applied to the flexural strength predictions of SCB tests. Actually, among several standardized tests for the

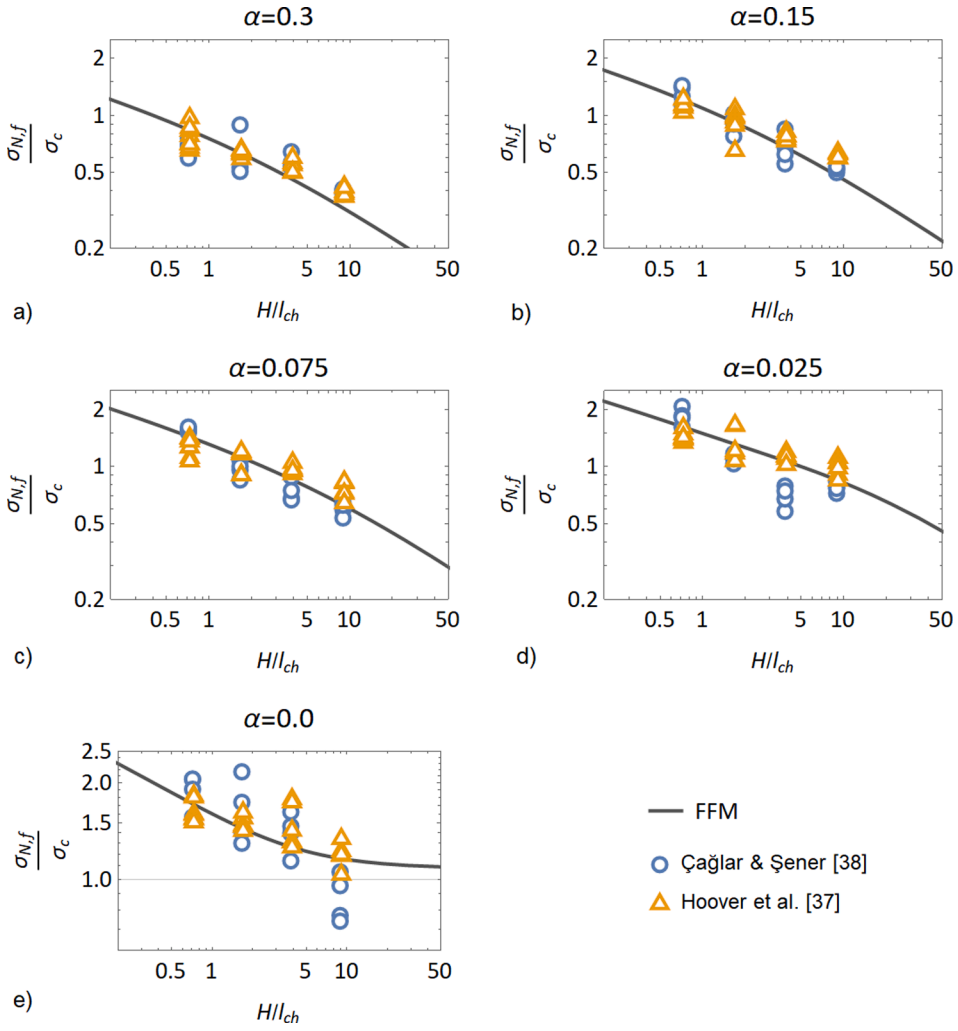

Fig. 11. Bi-logarithmic plots nominal failure stress vs specimen size for various relative crack depths: α = 30% (a), α = 15% (b), α = 7.5% (c), α = 2.5% (d), α = 0% (e). Lines refer to FFM predictions, markers to experimental values by Hoover et al. [37] (triangles) and by Çağlar & Şener [38] (circles).

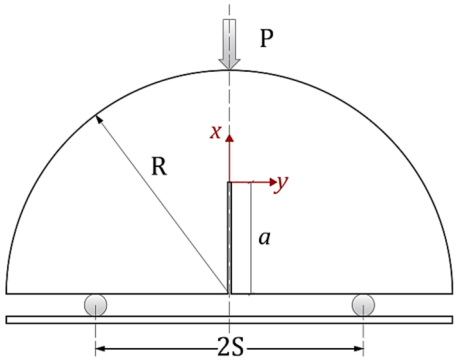

Fig. 12. SCB test set-up.

measurement of rock fracture toughness, the SCB test is quite popular and favorable, thanks to its simple sample preparation and testing procedure as well as the small amount of material required per specimen. Herein we briefly sketch the FFM solution, analogous to that presented in Section 4 for the TPB, and then skip to comparison with experimental data on rock specimens by Ghouli et al. [41].

5.1. Stress Intensity Factor

Fig. 12 shows a SCB specimen: B is the thickness, S the half span between supports, R the radius of the semicircular specimen and P the load applied at the specimen top. As already done for the TPB geometry, we introduce a slenderness index β defined as the ratio of half-span to radius (i.e., $\beta = S/R$) and the relative notch depth, here defined as the ratio of the crack length to radius $\alpha = a/R$ ($0 < \alpha < 1$). The origin of the reference system is placed at the crack tip.

Coherently with the notation used for TPB (Eq. (17)), we will write the SIF as:

$$K_I = \sigma_N \sqrt{R}\, f_k(\alpha, \beta) \tag{24}$$

where f_k is the shape function (of course different from the one holding for TPB – Eq. (18)) and:

$$\sigma_N = \frac{P}{2RB} \tag{25}$$

Note that in this case, differently from the TPB geometry, the nominal stress has no physical meaning, being just a reference stress value suitable for normalization purposes.

Although not as many as for the TPB geometry, some approximate analytical expressions for the shape function holding for the SCB geometry are available in the literature (Lim and Johnston [42], Kuruppu et al. [43], Ayatollahi et al. [44]). However, most of them hold only for a certain range of α values. This could lead to errors in the evaluation of the size effect by the FFM model, especially when looking at the small size asymptote, where the upper bound of the integral of the shape function tends to unity. To overcome this problem, we decide to numerically obtain the SIFs. We consider just the slender ratio $\beta = 0.6$, since it is the one of interest for comparison with experimental data. SIF values are determined by FEAs using a stress/displacement extrapolation technique, for α ranging from 0.1 to 0.9, increasing α by 0.05 at each step. Then we build the shape function f_k by interpolating the discrete values.

The shape function is plotted in Fig. 13 along with the analytical expressions by Ayatollahi et al. [44], which holds for $0.2 < \alpha < 0.8$ and $0.2 < \beta < 0.8$. The agreement is satisfactory, the difference being less than 6% for the relative notch depth analyzed in the present paper (i.e., for $\alpha = 0.5$). Nevertheless, in order to get more accurate and valid also in the small size limit results, we opt to exploit our numerically determined shape function, whose use is obviously restricted to the $\beta = 0.6$ case.

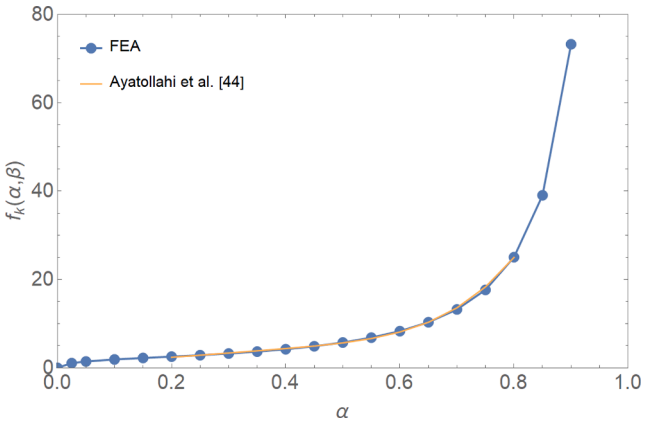

Fig. 13. Shape functions $f_k(\alpha, \beta)$ vs relative crack depth for $\beta = 0.6$.

Finally note that the shape function diverges (and the SIF does too) as the crack tends to cover the whole ligament.

5.2. Finite Fracture Mechanics

Provided that one replaces H with R (i.e., $\xi = x/R$, $\rho = R/l_{ch}$, $\delta = \Delta/R$), the FFM solution formally coincides exactly with the one holding for the TPB geometry, Eq.(23). What differ are just the shape functions f_σ and f_k. As before, the function f_σ is determined numerically (just one FEA was needed, since we considered only the *half-notched* geometry, $\alpha = 0.5$).

Provided that for the SCB test the nominal stress defined by Eq. (25) has no clear physical meaning and that we are considering the size effect just on cracked specimens, it is more interesting to highlight the size effect the *nominal* (or fictitious) fracture toughness is subjected to. This is readily achieved by substituting the latter equation of the system Eq. (23) into Eq. (24). Simple analytical manipulations yield the size effect on nominal fracture toughness in parametric form as:

$$\begin{cases} \rho(\delta) = \dfrac{\left[f_k(\alpha)\sqrt{2\delta/\pi} + \displaystyle\int_0^{\delta} f_\sigma(\alpha, \xi)\, d\xi \right]^2}{\delta \displaystyle\int_\alpha^{\alpha+\delta} f_k^2(\alpha')\, d\alpha'} \\ \dfrac{K_{IN,f}}{K_{Ic}}(\delta) = \dfrac{f_k(\alpha)}{\sqrt{\dfrac{1}{\delta}\displaystyle\int_\alpha^{\alpha+\delta} f_k^2(\alpha')\, d\alpha'}} \end{cases} \tag{26}$$

Note that the nominal fracture toughness can be seen as the (size-dependent) toughness value one should use in order LEFM to work at any scale. Furthermore, as the structural size grows, the finite crack increment Δ tends to be a material constant and, hence, $\delta = \Delta/R \to 0$; accordingly, the right-hand side of the second equation in Eq. (26) tends to unity and the nominal fracture toughness tends to the material one, as expected.

The two parametric size effect curves, Eq. (23) and Eq. (26), are plotted for the case $\alpha = 0.5$ geometry in Fig. 14a and Fig. 14b, respectively. Fig. 14a shows that the slopes of the small and large size asymptotes are the same as for TPB. On the other hand, Fig. 14b shows that the nominal fracture toughness is expected to increase with the size of the specimens by a (positive) slope $+1/4$ at small scales and then reaching a plateau for large scales, when the nominal fracture toughness tends to the material one (that is, K_{Ic}). It is clear that, wishing to determine the material fracture toughness by a single half-notched SCB test, it is required a radius of the specimen higher than 18 l_{ch}: beyond such a size, the expected difference between nominal and material fracture toughness is actually less than 5%.

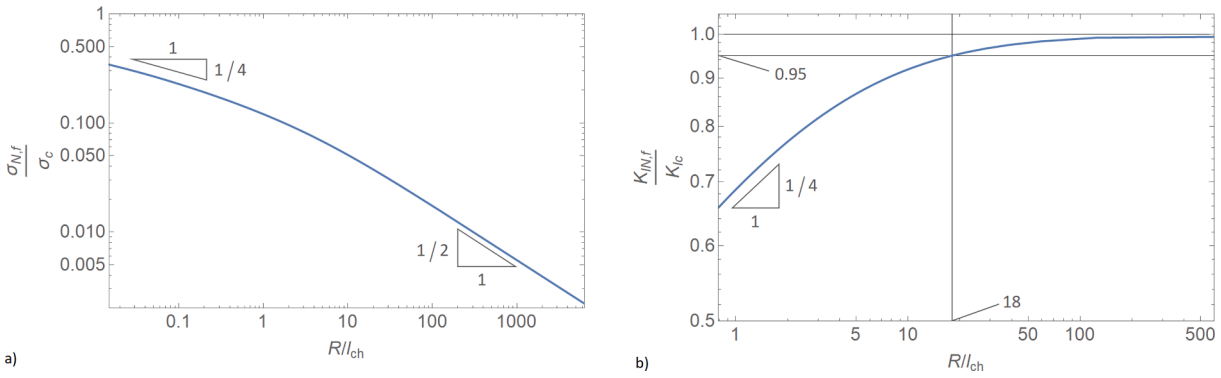

Fig. 14. Half-notched SCB tests: bi-logarithmic plots of size effect for on nominal strength (a) and fracture toughness (b).

5.3. Comparison with experimental data by Ghouli et al [41]

To check the reliability of our FFM approach to SCB modelling, we compare it with experimental data obtained by Ghouli et al. [41].

The research campaign by Ghouli et al. [41] consist in a total number of 93 SCB specimens, made of three different natural rocks: limestone, granite, and marble. The radii of the tested specimens were 25, 50, 75, 100, 150, 200 and 300 mm, thus covering a relevant size scale range, larger than one order of magnitude (1:12). The specimens were all half notched, i.e., $a/R = 0.5$, and with a thickness $B = 20$ mm, except the 300 mm radius specimen, for which a thickness of 30 mm was chosen in order to avoid buckling. The half span to radius ratio S/R was kept constant for all specimens and equal to 0.6. Finally, the Authors machined also cylindrical specimens and tested them to determine the splitting strength of the three different rocks. Note that tests were performed under vertical displacement control, which does not allow to monitor the post-peak behavior of the specimens, but the determination of the peak load was enough for our analysis.

In order to get FFM failure estimates, both K_{Ic} and σ_c are needed. When we apply the two-parameter least squares minimization procedure, we are not able to get a clearly defined minimum. Actually, we get a set of pairs of toughness and strength values minimizing the squares. From a physical point of view, it means that size effect data on just one (cracked) geometry is a too poor experimental dataset to get reasonable estimate for the two material parameters. Anyway, Ghouli et al. [41] also provided the splitting strengths, which we use as material tensile strength values. Once the σ_c values are fixed, for all the materials we applied the (one-parameter) least squares procedure yielding a well-defined minimum in correspondence of a particular K_{Ic} value, which we assume as the rock fracture toughness. Such values are reported in Table 1.

Fig. 15 shows the comparison between FFM predictions and experiments. It is worth observing that, since the plot is normalized, we are able to plot data, for the three rock types, on the same plot, the theoretical curve being unique. From Fig. 15, it is clear that FFM is able to catch satisfactorily the size effect on fracture toughness for all the three kinds of rocks. The matching is slightly worse for limestone, which show a less brittle behavior (l_{ch} is about twice the values for the other two rocks), and almost excellent for marble and granite. Note that for marble and granite the largest tested size have a radius close to 18 l_{ch} and thus, for that size, we expect a nominal fracture toughness close to the material one: actually, $K_{IN,f}$ is 1.53 MPa$\sqrt{m}$ for marble and 1.28 MPa$\sqrt{m}$ for granite, while the estimated K_{Ic} were 1.54 MPa$\sqrt{m}$ and 1.27 MPa$\sqrt{m}$ respectively.

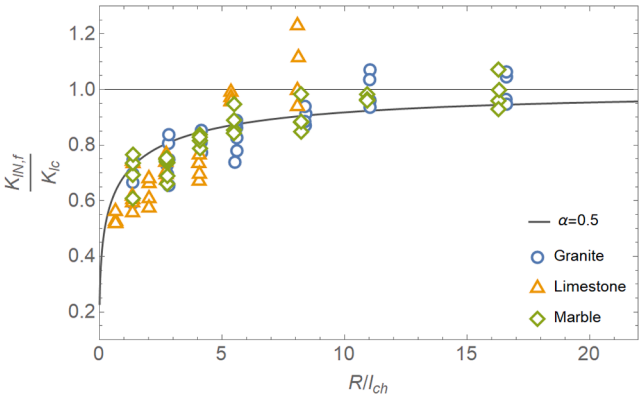

Fig. 15. Size effect on nominal fracture toughness for half notched SCB specimens. Comparison between FFM solution (solid line) and experimental data on rock specimens by Ghouli et al. [41].

6. Conclusions

Since its introduction, FFM has been applied to a variety of materials, geometries, loadings, and scales. However, one of its best performances is achieved in size effect investigation. In the present paper we applied FFM to investigate the size effect on the flexural strength of plain and notched specimens under bending loads. Particularly, TPB and SCB test geometries were analyzed and compared with several data from the literature on concrete and rock specimens.

Main conclusions are as follows:

- With respect to CCM, which requires an ad hoc simulation for each structural shape and size, FFM needs just one FEA per geometrical shape, providing the stress shape function, plus the SIF shape function providing the SIF for any crack length along the ligament. That is, two shape functions are enough to determine the scaling of the flexural strength over the whole range of scales.
- For plain specimens under pure bending, we obtained analytically the small and large size asymptotes. We also provided a master curve, that we hope to be useful in engineering practice to easily extract the material tensile strength from testing four-point bending specimens of different sizes.
- With respect to previous works on TPB and SCB test geometries, we highlighted that FFM size effect curve can be plotted without solving any transcendental equation, but just plotting it as a parametric curve where the parameter is the finite crack increment. This procedure largely simplified the problem and makes FFM approach even more attractive.
- Comparison with a relevant number of experimental size effect investigations on TPB concrete samples and SCB rock specimens was provided. The excellent agreement proved the soundness of the present approach.

Declaration of Competing Interest

The authors declare that they have no known competing financial interests or personal relationships that could have appeared to influence the work reported in this paper.

Data availability

Data will be made available on request.

Acknowledgements

Authors would like to thank Dr. Ghouli, Dr. Bahrami, Prof. Ayatollahi, Prof. Driesner and Dr. Nejati for their kindness and support in providing rough data of their experimental campaign on SCB rock specimens.

Appendix A

Here we provide the flexural strength size effect for plain specimens choosing the original FFM approach [5], i.e. Eq. (3). Upon substitution of Eq. (6) into (3) we get:

$$\begin{cases} \dfrac{\sigma_N}{\sigma_c} = \dfrac{1}{1-2\delta} \\ \left(\dfrac{\sigma_N}{\sigma_c}\right)^2 = \dfrac{\delta}{\rho \displaystyle\int_0^{\delta} f_{k\infty}^2(\alpha)\, d\alpha} \end{cases} \tag{A1}$$

Note that the second equation in system (A1) coincides with the corresponding one in Eq. (10), since the discrete energy balance remains unchanged. Starting from Eq. (A1) the size effect curve $\sigma_{N,f}/\sigma_c$ vs $\rho = H/l_{ch}$ can be given as a parametric curve where the dimensionless size and failure stress are expressed as a function of the parameter δ as:

$$\begin{cases} \rho(\delta) = \delta\, \dfrac{(1-2\delta)^2}{\displaystyle\int_0^{\delta} f_{k\infty}^2(\alpha)\, d\alpha} \\ \dfrac{\sigma_{N,f}}{\sigma_c}(\delta) = \dfrac{1}{1-2\delta} \end{cases} \tag{A2}$$

Differently from Eq. (12), where the parameter δ can vary only within the range (0, 1), in Eq. (A2) the range is (0, 1/2). This is because now the stress condition requires the stress to exceed the tensile strength over the whole crack advance and, thus, the finite crack growth is confined within the tensile zone (i.e. the specimen bottom half). Actually, $\delta \to 1/2$ defines the small size limit. Proceeding as in Section 3, the small size asymptote is easily achieved as:

$$\sigma_{N,f} = \frac{K_{Ic}}{\sqrt{2H \int_0^{1/2} f_{k\infty}^2(\alpha)\, d\alpha}} = 0.925 \frac{K_{Ic}}{\sqrt{H}}, \qquad H \to 0 \tag{A3}$$

Differently from Eq. (15b), the small size asymptote given by (A3) does not depend on the tensile strength. Moreover, note that the size effect provided by Eqs. (A2) and (A3) perfectly agrees with that obtained numerically by Doitrand et al. [26].

In Fig. A1 the size effect on flexural strength according to Eq. (12) and Eq. (A2) are compared. While the large size asymptote is the same (i.e. the tensile strength), it is apparent that the two FFM versions provide different results, especially for small sizes, where the slope in the bi-logarithmic plot is $-1/4$ for the average stress FFM approach and $-1/2$ for the original FFM formulation.

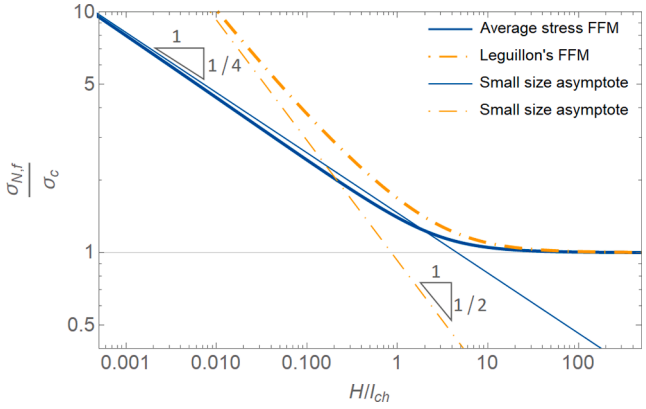

Fig. A1. Bi-logarithmic plot of size effect on flexural strength of plain specimens: a comparison between FFM results obtained by average stress FFM criterion (continuous line) and Leguillon's FFM formulation (dot-dashed line).

It can be easily shown that the aforementioned slopes remain unchanged also for TPB of notched/ unnotched specimens. In this sense, original FFM formulation provides a relatively strong size effect that does not fit properly the experimental data (on concrete) analyzed in the present paper. Of course, this observation does not imply that, for different materials or geometries, the original FFM could work properly.

References

[1] Z.P. Bažant, Size effect, Int. J. Solids Struct. 37 (2000) 69–80, https://doi.org/10.1016/S0020-7683(99)00077-3.

[2] V.V. Novozhilov, On a necessary and sufficient criterion for brittle strength, PMM 33 (1969) 212–222, https://doi.org/10.1016/0021-8928(69)90025-2.

[3] D. Taylor, The theory of critical distances, Eng. Fract. Mech 75 (2008) 1696–1705, https://doi.org/10.1016/j.engfracmech.2007.04.007.

[4] A. Hillerborg, M. Modeer, P.E. Petersson, Analysis of crack formation and crack growth in concrete by means of fracture mechanics and finite elements, Cem. Concr. Res. 6 (1976) 773–782, https://doi.org/10.1016/0008-8846(76)90007-7.

[5] D. Leguillon, Strength or toughness? A criterion for crack onset at a notch, Eur. J. Mech. A/Solids 21 (2002) 61–72, https://doi.org/10.1016/S0997-7538(01)01184-6.

[6] D. Leguillon, D. Quesada, C. Putot, E. Martin, Prediction of crack initiation at blunt notches and cavities - size effects, Eng. Fract. Mech. 74 (2007) 2420–2436, https://doi.org/10.1016/j.engfracmech.2006.11.008.

[7] G.H. Erçin, P.P. Camanho, J. Xavier, G. Catalanotti, S. Mahdi, P. Linde, Size effects on the tensile and compressive failure of notched composite laminates, Compos. Struct. 96 (2013) 736–744, https://doi.org/10.1016/j.engfracmech.2006.11.008.

[8] P. Cornetti, A. Sapora, A. Carpinteri, Mode mixity and size effect in V-notched structures, Int. J. Solids Struct. 50 (2013) 1562–1582, https://doi.org/10.1016/j.ijsolstr.2013.01.026.

[9] A. Doitrand, P. Cornetti, A. Sapora, R. Estevez, Experimental and theoretical characterization of mixed mode brittle failure from square holes, Int. J. Fract. 228 (2021) 33–43, https://doi.org/10.1007/s10704-020-00512-9.

[10] I.G. García, M. Paggi, V. Mantič, Fiber-size effects on the onset of fiber-matrix debonding under transverse tension: A comparison between cohesive zone and finite fracture mechanics models, Eng. Fract. Mech. 115 (2014) 96–110, https://doi.org/10.1016/j.engfracmech.2013.10.014.

[11] A.R. Torabi, S. Etesam, A. Sapora, P. Cornetti, Size effects on brittle fracture of Brazilian disk samples containing a circular hole, Eng. Fract. Mech. 186 (2017) 496–503, https://doi.org/10.1016/j.engfracmech.2017.11.008.

[12] T. Gentieu, J. Jumel, A. Catapano, J. Broughton, Size effect in particle debonding: Comparisons between finite fracture mechanics and cohesive zone model, J. Compos. Mater. 53 (2019) 1941–1954, https://doi.org/10.1177/0021998318816471.

[13] A. Chao Correas, M. Corrado, A. Sapora, P. Cornetti, Size-effect on the apparent tensile strength of brittle materials with spherical cavities, Theor. Appl. Fract. Mech. art. 103120 (2021), https://doi.org/10.1007/s10704-022-00655-x.

[14] P. Cornetti, N. Pugno, A. Carpinteri, D. Taylor, Finite fracture mechanics: A coupled stress and energy failure criterion, Eng. Fract. Mech. 73 (2006) 2021–2033, https://doi.org/10.1016/j.engfracmech.2006.03.010.

[15] Z.P. Bažant, J. Planas, Fracture and size effect in concrete and other quasi-brittle materials, CRC Press, 1997.

[16] Z.P. Bažant, Scaling of Structural Strength, Butterworth-Heinemann, 2005.

[17] Z.P. Bažant, Size effect in blunt fracture: concrete, rock, metal, J. Eng. Mech. 110 (1984) 518–535, https://doi.org/10.1061/(ASCE)0733-9399(1984)110:4(518).

[18] A. Carpinteri, B. Chiaia, G. Ferro, Size effects on nominal tensile strength of concrete structures: multifractality of material ligaments and dimensional transition from order to disorder, Mater. Struct. 28 (1995) 311–317, https://doi.org/10.1007/BF02473145.

[19] B.L. Karihaloo, H.M. Abdalla, Q.Z. Xiao, Size effect in concrete beams, Eng. Fract. Mech. 70 (2003) 979–993, https://doi.org/10.1007/s10704-008-9290-7.

[20] X. Hu, F. Wittmann, Size effect on toughness induced by crack close to free surface, Eng. Fract. Mech. 65 (2000) 209–221, https://doi.org/10.1016/S0013-7944(99)00123-X.

[21] J. Guan, X. Hu, Q. Li, In-depth analysis of notched 3-p-b concrete fracture, Eng. Fract. Mech. 165 (2016) 57–71, https://doi.org/10.1016/j.engfracmech.2016.08.020.

[22] J. Guan, X. Hu, X. Yao, Q. Wang, Q. Li, Z. Wu, Fracture of 0.1 and 2m long mortar beams under three-point-bending, Mater. Des. 133 (2017) 363–375, https://doi.org/10.1016/j.matdes.2017.08.005.

[23] J. Guan, Y. Yin, Y. Li, X. Yao, L. Li, A design method for determining fracture toughness and tensile strength pertinent to concrete sieving curve, Eng. Fract. Mech. 271 (2022), https://doi.org/10.1016/j.engfracmech.2022.108596.

[24] R. Louks, H. Askes, L. Susmel, Static assessment of brittle/ductile notched materials: an engineering approach based on the Theory of Critical Distances, Frat. ed Integrità Strutt. 8 (2014) 23–30, https://doi.org/10.3221/IGF-ESIS.30.04.

[25] P. Cornetti, M. Muñoz-Reja, A. Sapora, A. Carpinteri, Finite fracture mechanics and cohesive crack model: Weight functions vs. cohesive laws, Int. J. Solids Struct. 156 (2019) 126–136, https://doi.org/10.1016/j.ijsolstr.2018.08.003.

[26] A. Doitrand, R. Henry, S. Meille, Brittle material strength and fracture toughness estimation from four-point bending test, J. Theor. Comp. Appl. Mech., INRIA (2021) 1–17, https://doi.org/10.46298/jtcam.6753.

[27] G. Guinea, J. Planas, M. Elices, Stress intensity factor, compliance and CMOD for a general three-point-bend beam, Int. J. Fract. 89 (1998) 103–116, https://doi.org/10.1023/A:1007498132504.

[28] M.L. Williams, On the Stress Distribution at the Base of a Stationary Crack, J. App. Mech. 24 (1956) 109–114.

[29] Z.P. Bažant, Z. Li, Zero-brittleness size-effect method for one-size fracture test of concrete, J. Eng. Mech. (ASCE) 122 (1996) 458–468, https://doi.org/10.1061/(ASCE)0733-9399(1996)122:5(458).

[30] R. Ballarini, L. La Mendola, J. Le, A. Monaco, Computational study of failure of hybrid steel trussed concrete beams, J. Struct. Eng. (ASCE), 143 (2017), art. 04017060. doi:10.1061/(ASCE)ST.1943-541X.0001792.

[31] R. Ballarini, L. La Mendola, J. Le, A. Monaco, 2020, Computational assessment of the structural performance of concrete beams with encased steel joist. in: Proceedings of the 6th European Conference on Computational Mechanics: Solids, Structures and Coupled Problems, ECCM 2018 and 7th European Conference on Computational Fluid Dynamics, ECFD 2018, pp. 1187-1198.

[32] P. Colajanni, L. La Mendola, A. Monaco, Stress transfer and failure mechanisms in steel-concrete trussed beams: Experimental investigation on slab-thick and full-thick beams, Constr. Build. Mater. 161 (2018), https://doi.org/10.1016/j.conbuildmat.2017.11.134.

[33] P. Cornetti, A. Sapora, A. Carpinteri, Short cracks and V-notches: Finite Fracture Mechanics vs. Cohesive Crack Model, Eng. Fract. Mech. 168 (2016) 2–12, https://doi.org/10.1016/j.engfracmech.2015.12.016.

[34] A. Carpinteri, Size effects on strength, toughness and ductility, J. Eng. Mech. (ASCE) 115 (1989) 1375–1392, https://doi.org/10.1061/(ASCE)0733-9399(1989)115:7(1375).

[35] Y.N. Li, Z.P. Bažant, Eigenvalue analysis of size effect for cohesive crack model, Int. J. Fract. 66 (1994) 213–226, https://doi.org/10.1007/BF00042585.

[36] D. Grégoire, L.B. Rojas-Solano, G. Pijaudier-Cabot, Failure and size effect for notched and unnotched concrete beams, Int. J. Numer. Anal. Methods Geomech. 37 (2013) 1434–1452, https://doi.org/10.1002/nag.2180.

[37] C.G. Hoover, Z.P. Bažant, J. Vorel, R. Wendner, M.H. Hubler, Comprehensive concrete fracture tests: Description and results, Eng. Fract. Mech. 114 (2013) 92–103, https://doi.org/10.1016/j.engfracmech.2013.08.007.

[38] Y. Çağlar, S. Şener, Size effect tests of different notch depth specimens with support rotation measurements, Eng. Fract. Mech. 157 (2016) 43–55, https://doi.org/10.1016/j.engfracmech.2016.02.028.

[39] A. Carpinteri, P. Cornetti, A. Sapora, A Finite Fracture Mechanics approach to the asymptotic behaviour of U-notched structures, Fatigue Fract. Eng. Mater. Struct. 35 (2012) 451–457, https://doi.org/10.1111/j.1460-2695.2011.01637.x.

[40] Z.P. Bažant, E. Becq-Giraudon, Statistical prediction of fracture parameters of concrete and implications for choice of testing standard, Cem. Concr. Res. 32 (2002) 529–556, https://doi.org/10.1016/S0008-8846(01)00723-2.

[41] S. Ghouli, B. Bahrami, M.R. Ayatollahi, T. Driesner, M. Nejati, Introduction of a Scaling Factor for Fracture Toughness Measurement of Rocks Using the Semi-circular Bend Test, Rock Mech. Rock Eng. 54 (2021) 4041–4058, https://doi.org/10.1007/s00603-021-02468-1.

[42] I.L. Lim, I.W. Johnston, Stress intensity factors for semi-circular specimens under three-point bending, Eng. Fract. Mech. 44 (1993) 363–382, https://doi.org/10.1016/0013-7944(93)90030-VGet.

[43] M.D. Kuruppu, Y. Obara, M.R. Ayatollahi, K.P. Chong, T. Funatsu, ISRM-suggested method for determining the mode I static fracture toughness using semi-circular bend specimen, Rock Mech. Rock Eng. 47 (2014) 267–274, https://doi.org/10.1007/s00603-013-0422-7.

[44] M.R. Ayatollahi, E. Mahdavi, M.J. Alborzi, Y. Obara, Stress intensity factors of semi-circular bend specimens with straight-through and chevron notches, Rock Mech. Rock Eng. 49 (2016) 1161–1172, https://doi.org/10.1007/s00603-015-0830-y.